

Article

# Non-Contact Driver Respiration Rate Detection Technology Based on Suppression of Multipath Interference with Directional Antenna

Fan Yang <sup>1,2,\*</sup>, Zhiming He <sup>1</sup>, Shisheng Guo <sup>1</sup>, Yuanhua Fu <sup>1</sup>, Liang Li <sup>1</sup>, Junfeng Lu <sup>1</sup> and Kui Jiang <sup>1</sup>

<sup>1</sup> School of Information and Communication Engineering, University of Electronic Science and Technology of China, Chengdu 611731, China; zmhe@uestc.edu.cn (Z.H.); shishengG@std.uestc.edu.cn (S.G.);

f\_yuanhua@163.com (Y.F.); riemail@163.com (L.L.); luji2848@163.com (J.L.); 18847149074@163.com (K.J.)

<sup>2</sup> School of physics and electronic information, Inner Mongolia Normal University, Hohhot 010022, China

\* Correspondence: 201722020930@std.uestc.edu.cn; Tel.: +86-1855-0895-418

Received: 11 March 2020; Accepted: 3 April 2020; Published: 4 April 2020



**Abstract:** Non-contact driver respiration rate detection is a challenging problem in the Internet of Vehicles, because the automobile environment is much narrower, and thus the multipath effect is greater. To overcome these challenges, a 2.4 GHz continuous wave forward-scattering radar respiratory detection system is proposed based on the theory that the radar cross-section (RCS) of the human body changes with human breathing. We also analyze the impact of the multipath effect in the vehicle on the received radar signal and compare the output signal captured by a directional antenna with that captured by an omnidirectional antenna in the proposed system. In addition, the mean value of the received signal's envelope is used to judge whether the driver's posture is reasonable. Finally, compared with the existing contact respiratory detection system, the actual test results demonstrate the effectiveness of the proposed FSR system, and the driver respiration rates obtained by the proposed system are consistent with those obtained by the contact respiratory detection system.

**Keywords:** non-contact respiration detection; antenna; multipath effect; forward scattering radar

## 1. Introduction

The respiratory rate of drivers is an important index that reflects their physiological state. Effective detection of the driver's respiratory rate can provide important medical data support to recognize related scenarios of the driver, such as fatigue driving [1]. Valderas used heart rate variability analysis with spectral bands based on respiration to recognize human emotion [2]. Harold L. M. expounded that dyspnea is a cardinal symptom of asthma [3]. This means that breath detection is important for emotion recognition and for the detection of asthma. In the cognitive vehicle network architecture proposed by M Chen et al., physiological information monitoring of drivers plays an important role in safety application [4]. Similarly, non-contact breath detection for the driver can be integrated with the body sensor network (BSN) system and Internet of Healthcare thing (IoHT) system.

Generally speaking, the traditional respiratory rate detection uses contact respiration detection methods such as aerometer and respiration pectoral girdle. Although these methods have high detection accuracy, they require installing a contact sensor onto the human body, which brings inconvenience to use in practice. In addition, the unobvious contact sensor is also highly dependent on the cleanliness of the contact surface. Therefore, many non-contact respiration detection techniques, such as the thermal imaging method [5], machine vision analysis [6], and bio-radar [7,8] have been successively proposed. However, the above-mentioned methods cannot solve the respiration detection

problem well in the vehicle environment. For example, respiration detection is based on the thermal imaging method by using the thermal imaging camera to track the nostril from a proper angle in order to determine the adult's respiratory rate, but this method is severely affected by the object's body temperature. In the meantime, during human respiration, the temperature change is generally smaller than 1 degree Celsius [9,10], so it requires specialized thermal imaging equipment with high sensitivity, which involves high cost, and this will not benefit the automobile system. Furthermore, for the vision analysis method, the camera is significantly influenced by illumination. Such sufficient light cannot be obtained during night driving, so it requires artificial illumination, which will heighten risk of a traffic collision or accident. Therefore, non-contact respiration detection based on bio-radar is a powerful technique for the respiration detection of the driver. Mehrotra summarized the EM-Wave Biosensors including microwave and mm-wave [11]. In general, there are two types of bio-radar: ultra-wideband bio-radar (UWB) [12–14] and continuous wave radar [15,16]. UWB has a large bandwidth and small power consumption. However, it involves complex hardware design and high overall cost. In 2010, Levitas used UWB radar to realize live person detection behind non-metallic obstacles [17]. In 2018, Schires proposed installing UWB in the driver's seat, which can accurately detect the respiration and heart rate, but it still has the problem of high cost and increases error caused by motion artifact and clothes [18]. In comparison, since it is unnecessary to consider the requirements of high switching speed and high delay precision of an integrated chip in a UWB radar system, continuous wave (CW) radar has a simpler structure. Pisa proposed a double-sideband CW radar system to detect the carotid wall movement in 2018 [19]. However, when the phase constant is equal to integer times of  $\pi$  in a traditional CW radar system, the phase change in demodulation will not be linearly related to the displacement change, resulting in the decrease of precision (the zero-phase problem).

In order to detect the driver's respiratory rate in the vehicle, it not only requires solving the adaptability problem of bio-radar, but it also needs to reduce the system cost. In 2015, Wu et al. proposed the technology of using a WiFi signal to detect human respiration, which greatly reduced the cost of the non-contact respiratory detection system [20]. However, the environment of cars is narrow for the sake of the strong multipath effect, and the performance of the respiratory detection was poor.

In summary, the respiration rate detection technology of bio-radars should be accurate, the multipath effect should be brought down, and the hardware should be low cost. In addition, judging whether the driver's posture is reasonable is the icing on the cake.

The main contributions of this paper can be summarized as follows:

1. To achieve the driver's respiration rate in car, we propose a continuous wave respiration detection system based on the forward scattering radar. The main idea of the proposed method is that during the respiration process, the changes of body contour will change the radar cross-section (RCS), which will further affect the amplitude of the received signal.
2. To suppress the multipath interference, we use a directional antenna instead of an omnidirectional antenna. The experimental results show that the performance obtained by a directional antenna is superior than that obtained by an omnidirectional antenna.
3. By computing the mean value of the received signal's envelope, we can judge whether the driver sitting posture is reasonable.
4. We have designed the whole non-contact respiration detection system and finished the comparative experiment with a contact respiration detection system. The experimental results show that the non-contact respiration detection system can output accurate test results. However, it is sensitive to road conditions.

## 2. Detection Principle and Theoretical Model

During the respiration process of the driver, the driver's diaphragm makes contraction and relaxation movements, which changes the chest volume. As the diaphragm contracts, the volume of the thoracic cavity increases, thereby creating a negative pressure, which draws air into the lungs. The movement of these organs directly changes the contour of the human body, causing the changes of

RCS. This will further trigger the change in the amplitude of the received signal, so that an effective respiration feature can be extracted from the received signal, and the respiratory rate can be obtained through peak detection.

The forward-scattering radar (FSR) is a bistatic radar system with bistatic angle approaches to  $180^\circ$ . In recent years, it has attracted broad attention from both the industrial and academic fields. It was widely used in vehicle detection [21] and through-the-wall human motion sensing [22]. When the bistatic angle is higher than  $180^\circ$ , its RCS will rapidly increases. On the other hand, when the bistatic angle is  $180^\circ$ , RCS depends on the projected outline of the electric conductor and the length of the electromagnetic wave, which is not related to the wave-absorbing characteristic of the target. So, in this paper, we have studied and verified the principle of forward-scattering radar in human respiration and proved that the FSR system has good robustness for different clothing and antenna irradiation angles in breath detection application [23]. Essentially speaking, the 2.4 GHz incident wave mainly penetrates the clothing rather than reflects or absorbs it. The reflection and absorption of the clothing is far less than the reflection and absorption of the human body. This is the reason why the FSR system is insensitive to clothes. Furthermore, for most of the reflection-based bio-radars, the respiration detection is conducted according to the change of micro-Doppler signature caused by the small movement of the chest wall. In our work, the FSR radar is employed to explore how the amplitude of the received signal changes with the respiration of the human body within the vehicle. Figure 1 shows the FSR radar system.

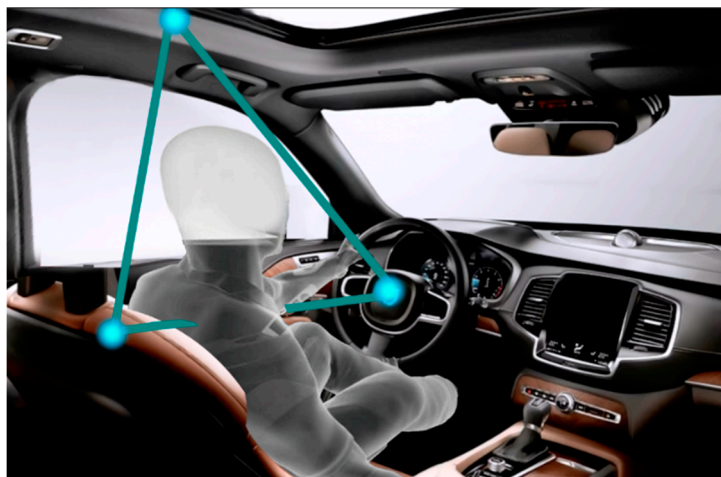


Figure 1. Driver's respiration detection system.

As shown in Figure 1, we ignore the scattering field generated by the current on the human body surface and the electromagnetic wave penetrating the electromagnetic field of human body. So, we have

$$\mathbf{E}_r = \mathbf{E}_t - \mathbf{E}_{body} + \mathbf{E}_{en} \quad (1)$$

where  $\mathbf{E}_r$  is the electric field at the receiver;  $\mathbf{E}_t$  is the electric field of the transmitted signal on the surface of the human skin;  $\mathbf{E}_{body}$  is the shadow field caused by the blocking of the human body; and  $\mathbf{E}_{en}$  is the electric field generated by the environment reflection. Since the transmitter has fixed power,  $\mathbf{E}_t$  is fixed. In addition, the environment under the vehicle does not change, and when only considering the environment reflection of the transmitted signal,  $\mathbf{E}_{en}$  is also fixed. In Equation (1),  $\mathbf{E}_{body}$  is directly affected by the change of the human body's RCS. When the bistatic angle approaches  $180^\circ$ , according to the RCS, denoted by  $\sigma_b(180^\circ)$ , which is the computational formula proposed in the far-field condition [24], we can obtain:

$$\sigma_b(180^\circ) = 4\pi \left( \frac{S_t}{\lambda} \right)^2 \quad (2)$$

Here,  $\lambda$  is the wavelength of the transmitting signal, and  $S_t$  is the projected area of the target in the direction of the incident wave.

In the near-field condition, by dividing the human chest into several polygonal plane elements of small size, in which each plane element satisfies the far-field condition, and considering the influence of antenna directivity factor on the near-field, the total near-field RCS  $\sigma_\Sigma$  of the target can be obtained. Chen proposed Formula (3) [25],

$$\sigma_\Sigma = \left| \sum_{n=1}^N f(\theta, \varphi) \sqrt{\sigma_n} \exp\left(\frac{i4\pi(\mathbf{o} - \mathbf{i}) \cdot \mathbf{R}_n}{\lambda}\right) \exp(i\phi_n) \right|^2 \tag{3}$$

$\mathbf{O}$  is the unit vector of the scattering direction,  $\mathbf{i}$  is the unit vector of the incident direction,  $f(\theta, \varphi)$  is the antenna’s directivity factor,  $N$  is the total number of plane elements,  $\mathbf{R}_n$  is the position vector of the scattering center of the  $n$ th plane element, and  $\exp(i\phi_n)$  is the phase factor of the plane element  $n$  relative to the reference phase center. When a person inhales, the chest cavity gets bigger and  $N$  increases. This leads to a larger RCS, which makes the amplitude of the received signal smaller. In contrast, when a person exhales, the chest cavity shrinks. This leads to a decrease in the RCS, which makes the amplitude of the received signal bigger. Throughout the respiratory cycle, the amplitude varies with the respiration. Using this principle, the rate of breathing can be measured.

### 2.1. Multipath Problem and Antenna

Figure 2 shows the multipath effect in a car. In Figure 2, A is the location of the transmitter; B is the location of the back seat; C is the body of the driver; D is the location of the receiver; and E is the top of the car. For FSR, the transmitter transmits a single-frequency continuous wave signal, and the signal model can be expressed as:

$$T(x) = A \cos(\omega t + \varphi) \tag{4}$$

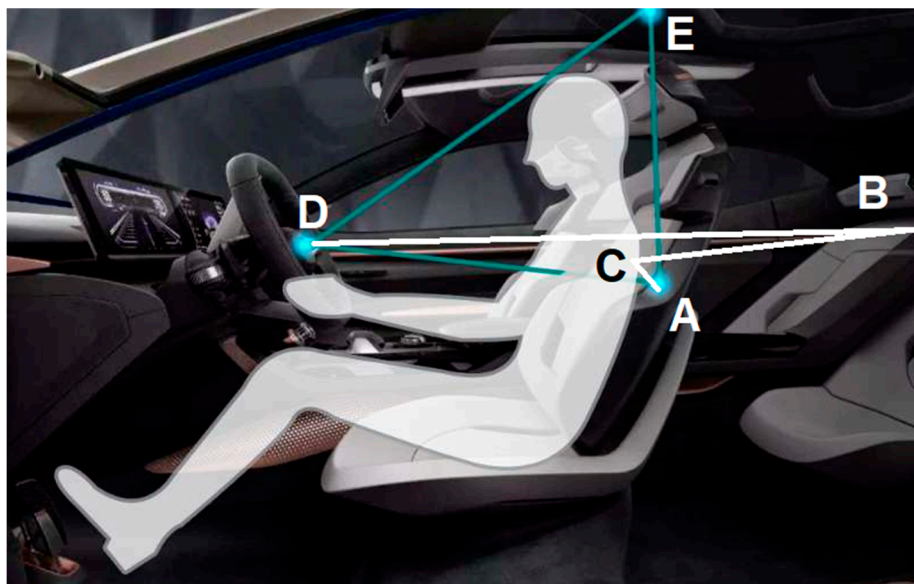


Figure 2. Multipath analysis diagram.

According to Formula (1), the amplitude  $A$  of carrier signal becomes  $A(t)$ , which changes with time due to the influence of human respiration, and  $A(t)$  is also affected by the environment within the vehicle. As shown in Figure 2, the environment influence  $E_{en}$  consists of two parts: one part is the reflection electric field  $E_0$  without respiration information; the other part is the electric field  $E_{multipath}$

with respiration information after reflection by human body. Since the environment under the vehicle is approximately fixed,  $E_0$  is also fixed.

$$A(t) = A_0 - A_{body}(t) + A_{multipath}(t) \quad (5)$$

where  $A_0$  is the constant amplitude, which depends on the transmitter's transmitting power and vehicle environment;  $A_{body}(t)$  is the carrier amplitude of the shadow field caused by blocking during the respiration process of the human being, which carries the respiration information; and  $A_{multipath}(t)$  is the multipath effect and interference caused by the vehicle environment. During the respiration process, a person's abdomen will become bigger when breathing in, the projected area will increase,  $A_{body}(t)$  will increase too because it is in direct proportion to the square of the projected area, and according to Formula (6), the amplitude of a received signal will decline. On the contrary, a person's abdomen will become smaller when breathing out, the projected area decreases,  $A_{body}(t)$  also decreases, and according to Formula (6), the amplitude of received signal will increase. Based on the above theoretical analysis, it can be seen that the contour of the human body will change during the respiration process. Thus, the human body conducts the amplitude modulation of the radio signal, and the respiratory rate of the human body can be detected by designing a low-cost amplitude demodulation circuit.

In order to reduce the multipath effect on the system, the reasonable electromagnetic wave path must be designed, and the electromagnetic wave path should be considered from the antenna installation and radiation pattern. Gouveia discussed different antenna designs for non-contact vital signal measurements, and the directivity and gain of antennas were proved to be very important in the system [26]. It was proved by many applications; for example, Comite used a directional wideband antenna to gather ground-penetrating radar data [27].

Firstly, the position of the antenna. Since the forward scattering radar is highly sensitive to the contour of shielding the conductor, there can be no conductor shielding within the radiation range of the antenna. Therefore, we set the transmitter antenna in the driver's seat and the receiver antenna on the steering wheel, so that the signal field from transmitting to receiving covers the human chest.

Secondly, the distance between the driver's back and the seat is random, so the distance between the back and the seat should be at least 0 cm when the back is in contact. Therefore, as shown in Figure 2, it is necessary to adopt a directional antenna in the transmitter antenna, to make the wireless electromagnetic wave diffraction and penetration through the body in the A-D route, and the multi-path scattering route is A-C-B-D. The useful signal and the multipath signal transmit distances, the amplitude of the radio signal fading is different, so that the system can easily distinguish between respiratory signals and multipath interference.

$$Lbf = 32.44 + 20lgd + 20lgf \quad (6)$$

where  $Lbf$  is the free space loss of the radio, its unit is dB,  $d$  is the radio signal transmitting distance, its unit is km,  $f$  is the frequency of the carrier.

$$RSS = Pt + Gr + Gt - Lc - Lbf \quad (7)$$

$RSS$  represents the received signal strength,  $Pt$  is the transmit power of the radio signal,  $Gr$  is the receive antenna's gain,  $Gt$  is the transmit antenna's gain, and  $Lc$  is the attenuation of the cable and cable head. Formula 8 shows that  $RSS$  is only affected by  $Lbf$ , due to  $Pt$ ,  $Gr$ ,  $Gt$ , and  $Lc$  being constant, and  $Lbf$  is also affected by transmission distance  $d$ .

## 2.2. Driver Posture

Figure 3 shows the sitting posture of the driver, as shown in Figure 3a, which is a common wrong sitting posture. The sitting posture of the novice driver is closer to steering wheel, which makes the

body stiff, easily tired, and difficult to move in emergency. Figure 3b shows the right sitting posture of the driver, which is relatively relaxed for drivers.

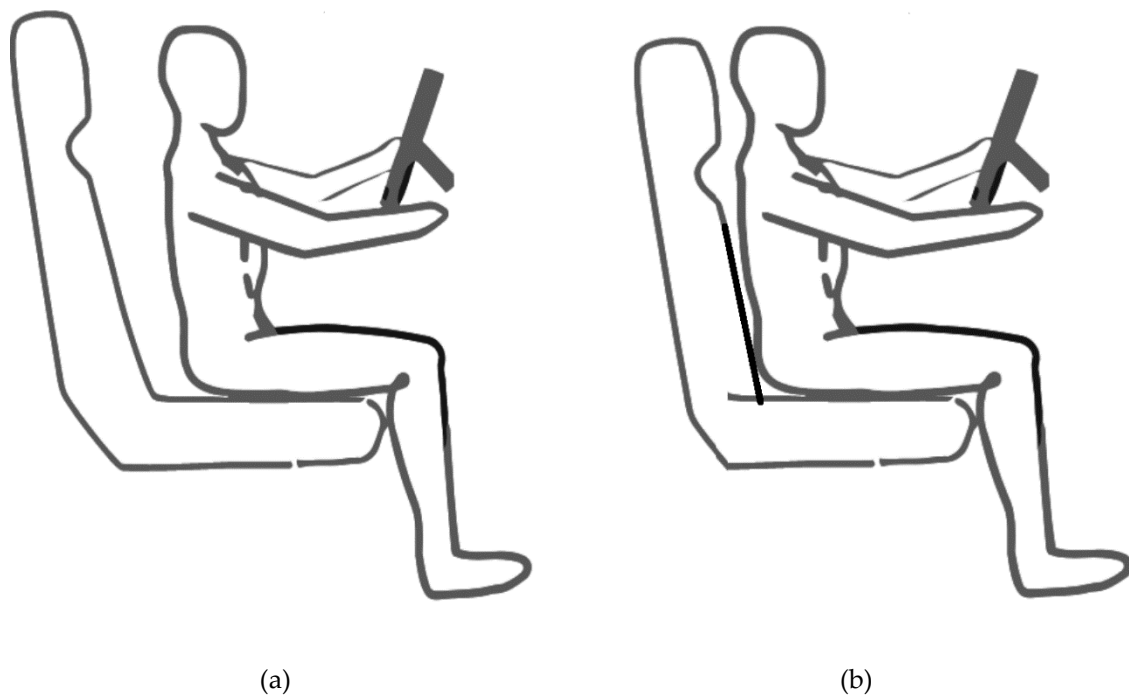


**Figure 3.** Driver sitting posture: (a) wrong posture; (b) right posture.

For forward-scattering radar, the sitting status of the driver can be obtained from the mean of the received signal envelope. When the back of the driver touches the seat, most of the transmitting signals are blocked, and the mean of the envelope of the received signal becomes smaller. When the driver's back leaves the seat, the transmitting signal diffuses through the body, and the mean value of the received signal's envelope increases.

### 3. Experiment and Analysis

First of all, the system setup is shown in Figure 4, and the system block diagram is shown in Figure 5. As the transmitter controller, the STM32F103SCM sends the configuration information to HMC830 through the Serial Peripheral Interface (SPI) bus; then, HMC830 generates a 1 dBm 2.4 GHz single-frequency continuous wave signal; after the signal is amplified, the 2.4 GHz single-frequency continuous wave signal is sent to the human body via the directional antenna; the electromagnetic wave has diffraction after passing through human body, and after it reaches the receiver antenna, the received radio signal will be amplified to be above  $-10$  dBm. Then, the system executes envelope detection via ADL5511, and the output low-frequency signal is amplified to the analog-to-digital conversion (AD) sampling range of 0–5 V; next, Arduino sends the digital sampling information through the USB interface to the computer for analysis. During the system work, we also employ the RSA306B spectrum analyzer to analyze the components of the received signal.

In the meantime, the contact piezoelectric sensor IM-9006B based on PVDF (polyvinylidene fluoride) was fixed on the chest of the test object to compare the accuracy of the detection system. As shown in Figure 4, A is the transmitter antenna, B is the receiver antenna, and C is the PVDF sensor.

We finished four experiments in the environment as follows.



**Figure 4.** Experiment setup in car.

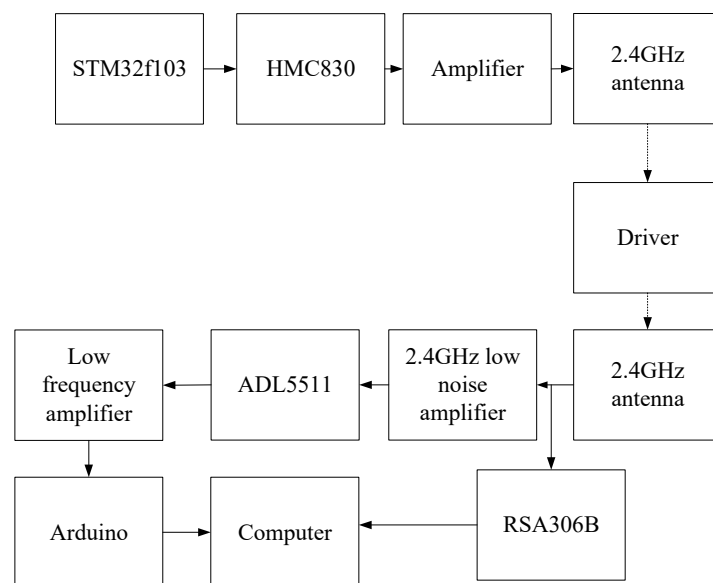


**Figure 5.** The experiment system block diagram.

### 3.1. Experiment 1: Antennas Comparison

Firstly, we test different antennas in the system to compare their performance. The experiment is executed in a Chevrolet Cruze vehicle manufactured in 2017, and both the transmitting antenna and receiving antenna are 2.4 GHz directional antennas. The transmitting antenna was installed on the seat of main driver, and the antenna is radiated onto the back of the human body. The receiving antenna was installed on the steering wheel. The test object simulated the posture of operating the steering steel during the test. We tested the directional antenna and the omnidirectional antenna respectively under the same system. The details of the directional antenna are shown in Figure 6, and we can find that its 3 dB beam width is  $66^\circ$ . The details of the omnidirectional antenna are shown in Figure 7. The directional antennas belonged to the Jiayuan series, which was offered by Xinshengfa Technology Company in Shenzhen. The nondirectional antennas were manufactured by Tp-link company in Shenzhen.

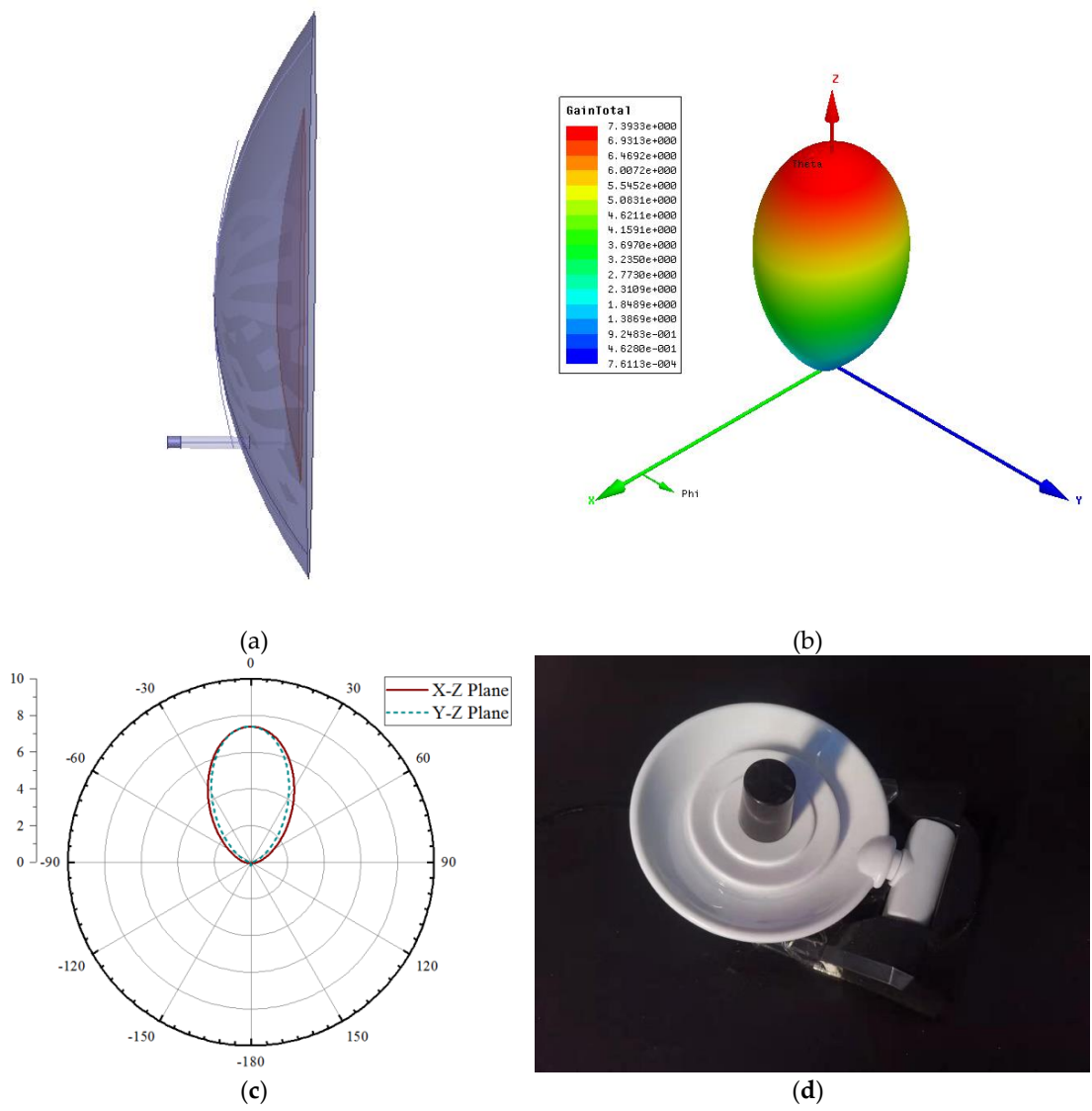


**Figure 6.** The directional antenna information: (a) the antenna model; (b) the antenna radiation in 3D; (c) the antenna radiation; (d) the antenna prototype.

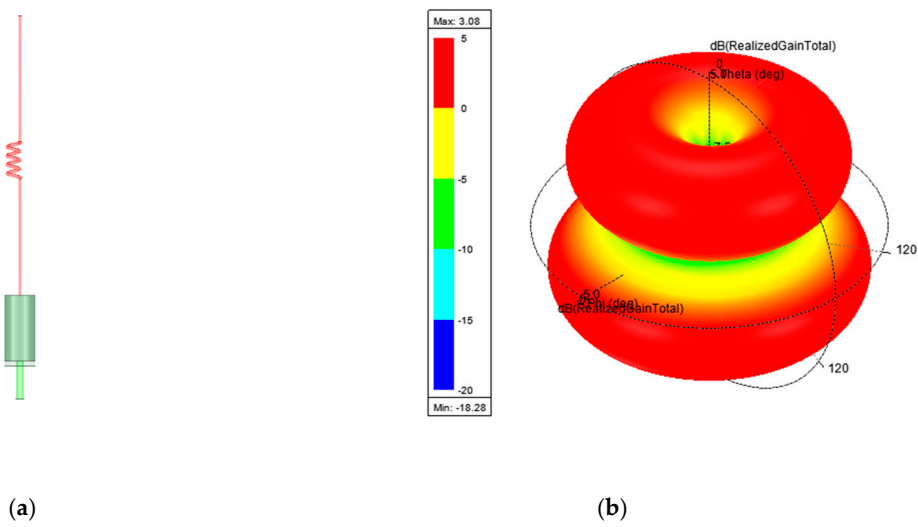
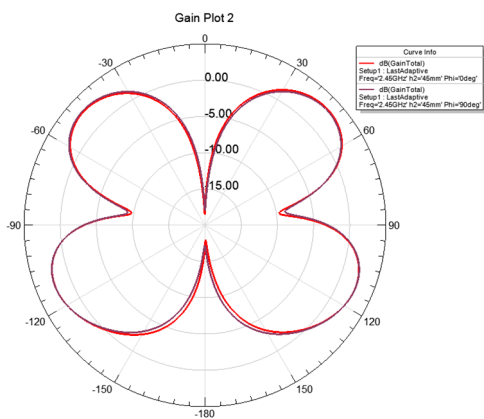


**Figure 7.** Cont.



(c)



(d)

**Figure 7.** The nondirectional antenna information: (a) the antenna model; (b) the antenna radiation in 3D; (c) the antenna radiation; (d) the antenna prototype.

Figures 6 and 7 show the two kinds of antennas that were used in the experiment. Directional antennas achieved better performance than the nondirectional antennas because the signal power of directional antennas are more concentrated, which helps to reduce the influence of the multipath effect.

Figure 8 shows the raw received signal with a nondirectional antenna, and Figure 9 shows the raw received signal with a directional antenna. As shown in Figure 9, we can clearly find that the signal with respiration information was greatly affected by multipath effect in the system with a nondirectional antenna. It is difficult to acquire the respiration information from Figure 8. On the other hand, we can find that the respiration change caused the change of the received signal amplitude. The results show that the directional antenna is more suitable for in-car respiration measurements.

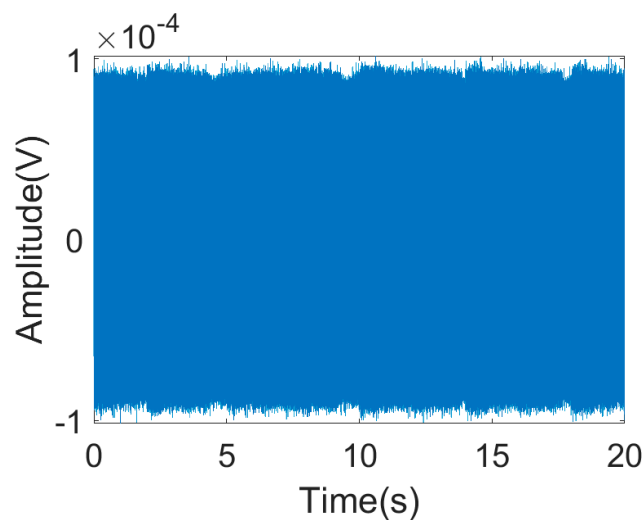


**Figure 8.** The output with a nondirectional antenna.

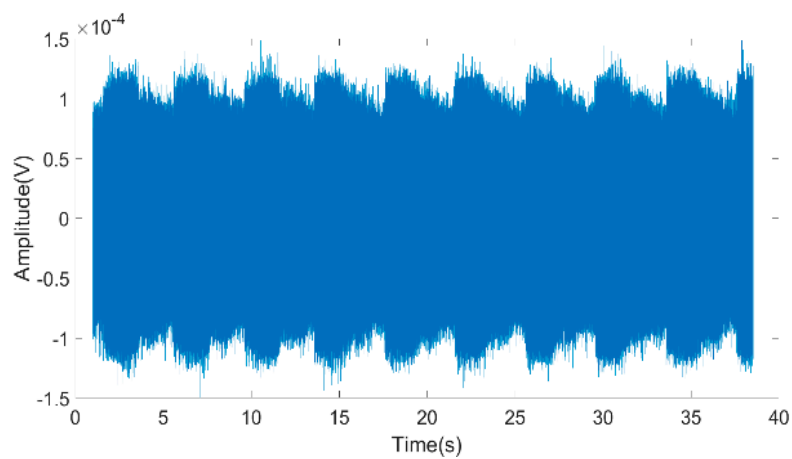


**Figure 9.** The output with a directional antenna.

### 3.2. Experiment 2: Driver Sitting Posture Test

In this part, we used the same setup as that with Experiment 1 and finished the experiment in 140 s with a directional antenna. During the process of the experiment, the testee changed their sitting posture. Figure 10 shows the raw received signal. Figure 11 shows the envelope of Figure 10.

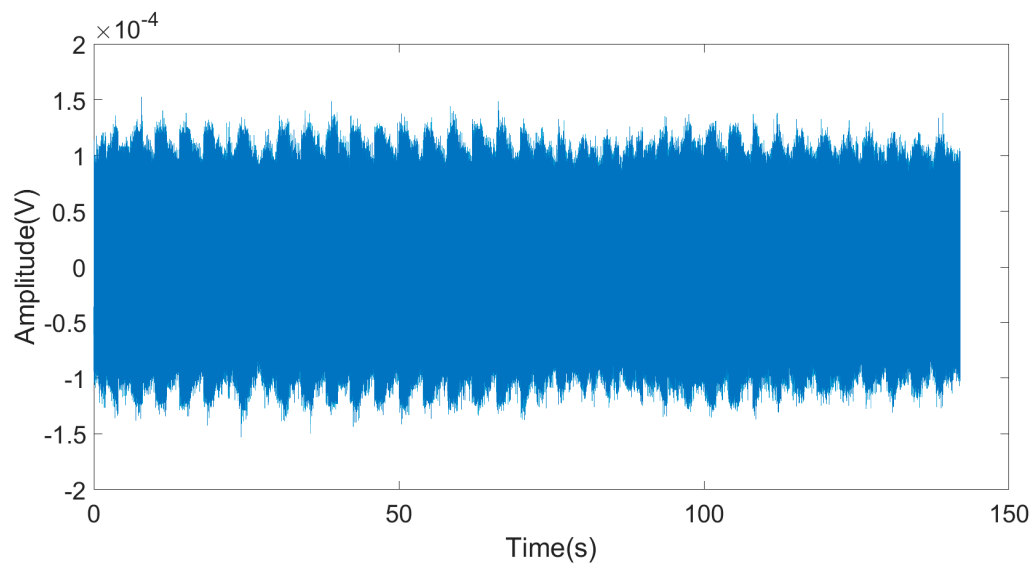


**Figure 10.** The raw received signal with directional antennas.

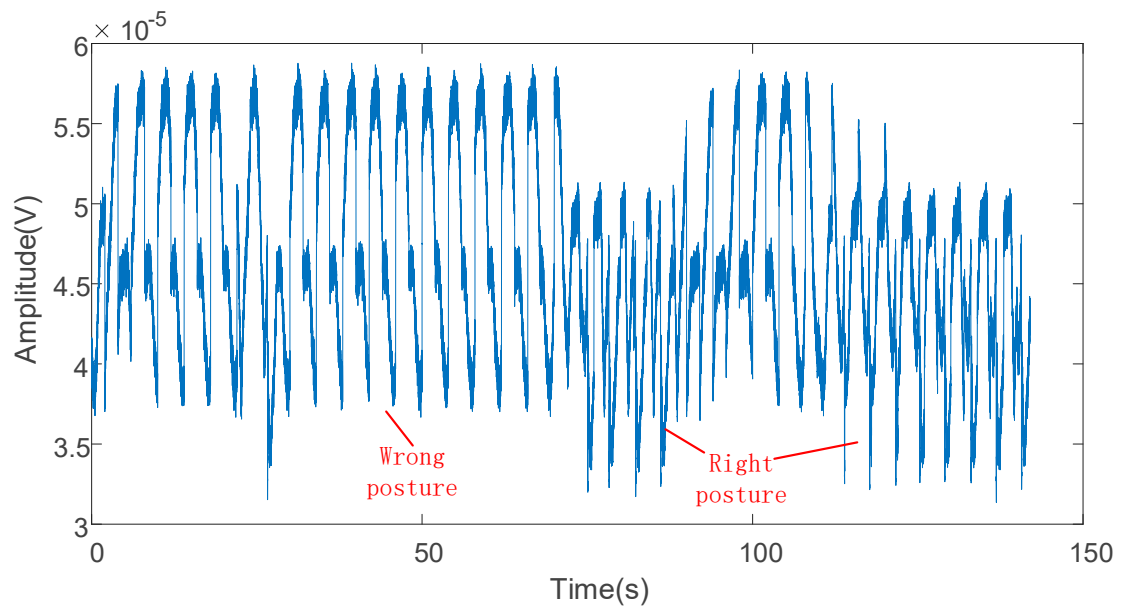


**Figure 11.** The envelope of the received signal.

In Figure 11, we can see that when the testee sat in the wrong posture, the mean value of the received signal envelope was greater. Furthermore, we segmented the envelope data every 4 s. The result is shown in Figure 12, and we can easily set a threshold to classify the driver’s sitting posture.

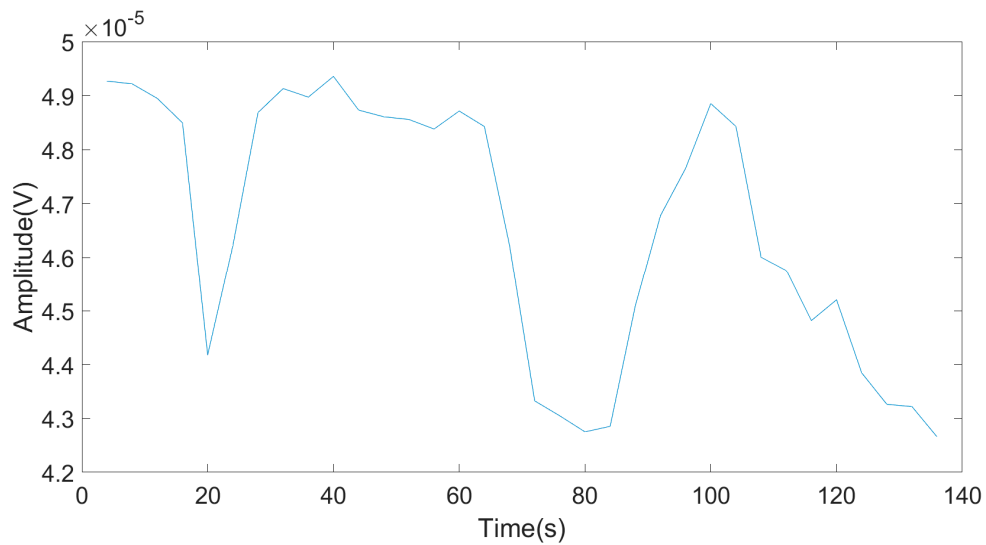


**Figure 12.** The mean value of the segment.

### 3.3. Experiment 3: Driver’s Respiration Detection by FSR System Compared with PVDF Sensor

Finally, to confirm the accuracy of the respiration detection technology, we plugged the PVDF sensor into the system, and the Arduino flow chart is shown in Figure 13.

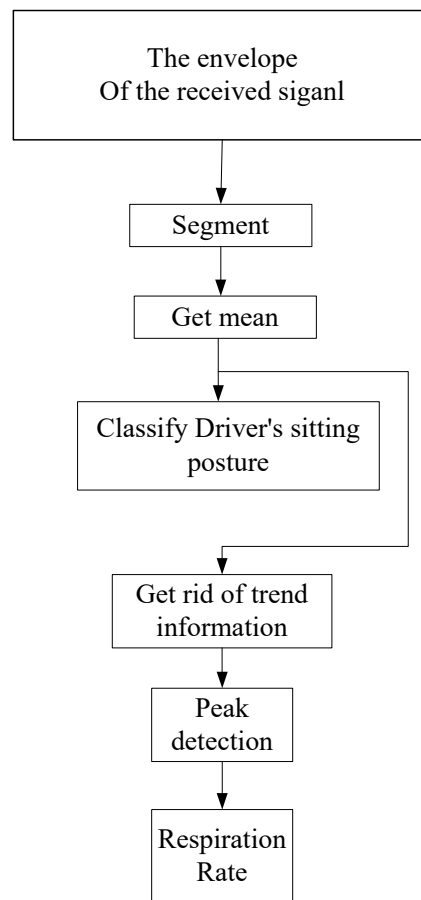
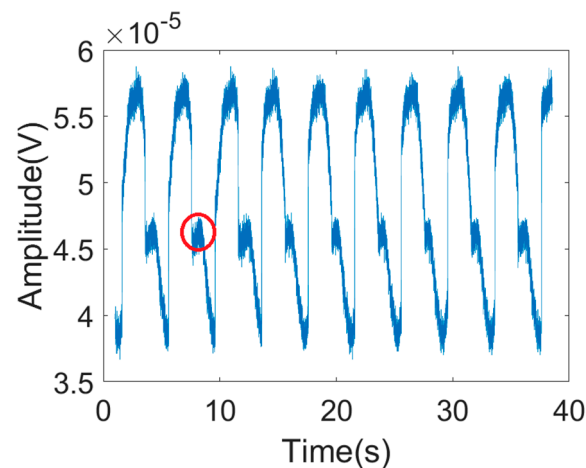


Figure 13. The Arduino flow chart.

In Figure 13, the system obtained the discrete envelope signal with the 10 kbps AD sample rate. Then, the signal was segmented every four seconds, and the average value of each segment was calculated, so that the sitting position of the driver could be determined. At the same time, by using the average value obtained in sections and removing the trend information, a stable respiratory curve could be obtained. By the peak detection algorithm, we could calculate the peak number, denoted by  $N$ , of the curve. Furthermore, each peak corresponds to a respiratory cycle, and we can calculate the respiratory rate as  $RR = N/timelength$ , in which  $RR$  denotes the respiration rate and  $timelength$  denotes the test time with the unit of minute.

As shown in Figure 14, after the receiver receives the electromagnetic signal with an amplitude change, the amplifier and filter are used to maximally reduce the interference from the other frequency bands. Then, envelope detection is conducted to the signal. Envelope detection is a common demodulation method for amplitude-modulated signals, which involves very low hardware realization cost. Figure 14 shows the results of the envelope detection. According to Figure 14, it can be seen that the received signal is not an ideal sine wave signal, which has partial distortion; the reason is that this partial distortion is caused by the multipath effect within the vehicle. Since the transmitter uses a directional antenna, most multipath signals are reflected to the rear part of the vehicle from the back of human body before entering the receiver. Therefore, setting the transmitter on the back of the human body and the receiver antenna on the steering wheel can effectively reduce the influence of multipath effects.



**Figure 14.** The output with a directional antenna.

Furthermore, according to Figure 9, the received signal is an amplitude modulation signal. When breathing in, the RCS of the human body decreases, the number of blocked radio signals declines, and the received signals becomes bigger; on the contrary, when a person breathes out, the RCS of the human body increases, the blocked radio signal becomes greater, and the received signal becomes smaller. No matter the angle of the person corresponding to the antenna, the way that the change of respiration affects the change of RCS remains the same, and what is changed is the overall amplitude. In addition, according to Figure 14, we can see that the respiration curve is not a standard sine wave but rather a waveform with certain distortion, which also verifies the influence of the multipath effect on the detection system. From Figure 13, it can also be seen that the multipath effect only has a limited impact on the detection performance, which also verifies our previous analysis.

Figure 15 compares the results of the PVDF sensor to our proposed system. It can be seen that although the curve of the PVDF sensor does not completely coincide with the output curve of our proposed FSR, the number of the curve peaks detected by the FSR system is the same as that with the PVDF system. During the 38-s test, 10 respirations were completed in total, so the respiration rate was 15.8 per minute.

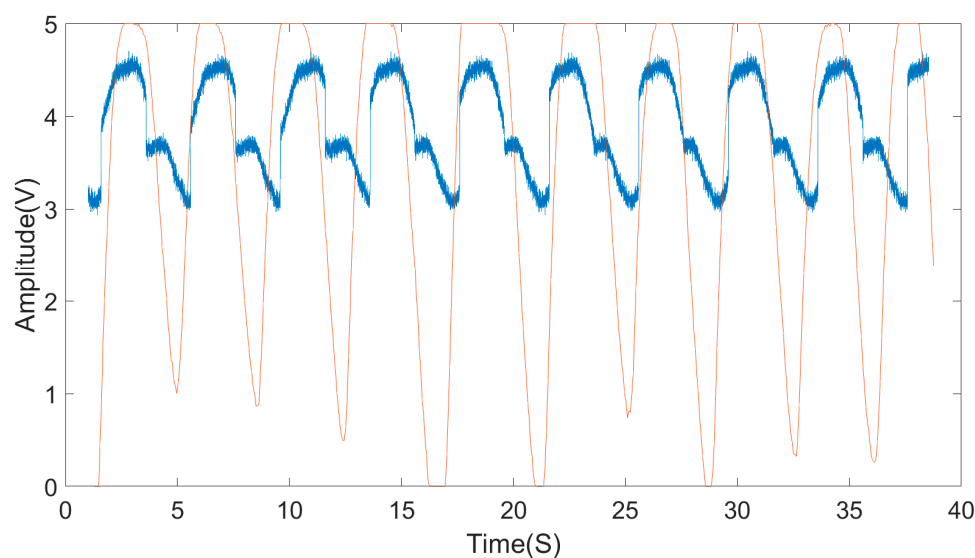


**Figure 15.** The output with a directional antenna compared with a polyvinylidene fluoride (PVDF) system, in which the red line is the output of the PVDF system.

To test the robustness of the system, we tested 3 testees breathing in for 30 s with the same setup, and the results are shown in the Table 1. The relative error of the system is shown in Formula (8).

$$\text{Relative Error} = \frac{|FSR - PVDF|}{PVDF} \quad (8)$$

**Table 1.** Comparison of PVDF system and forward-scattering radar (FSR) system.

Subjects	Age	PVDF (times)	FSR (times)	Relative Error
A	35-year-old	10	10	0%
B	62-year-old	12	11	8.33%
C	25-year-old	9	9	0%

From the experimental results, we can find that the system error increases when testing the elderly, which is caused by the random movement of the testees.

#### 3.4. Experiment 4: Breath Detection on Bumpy Roads

To observe the robustness of the system on bumpy roads, we completed the respiration rate detection experiment on a bumpy road, for which the car we used was a Toyota Corolla, manufactured in 2012. This experiment setup is similar to that in Experiment 3. The testee is 62 years old and weighs 61 kg. Figure 16a shows the test environment inside the car. A is the directional receiver antenna, B is the directional transmitter antenna, and C is the PVDF sensor. As shown in Figure 16b, the road is a cement and gravel road with pits.



**Figure 16.** The experiment setup: (a) the experiment inside the car; (b) the experiment road.

Since the PVDF sensor is not accurate in the process of car bumping, we asked the testee to count the number of breaths within 30 s during the experiment. The result is shown in Figure 17a,b. Figure 17a is the raw radio wave. Furthermore, during the process from A to B in Figure 17a, the mean value of the signal decreased, because the car shaking caused a change in the subject's sitting posture. Figure 17b is the envelope of the received signal, and we used a peak detection algorithm with the minimum peak interval of 1.5 s. Throughout the test, there was a lot of high frequency vibration in the waveform of Figure 17a,b, which may make the system mistakenly think that respiration rate increases. As a result, we reduced the influence of the high-frequency vibration by setting the peak interval.

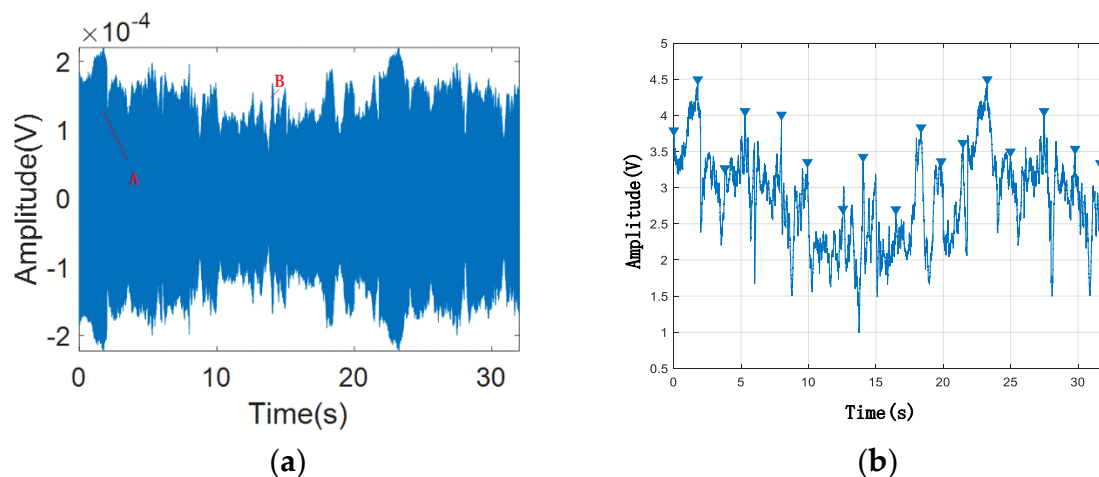


**Figure 17.** The output of the received signal with directional antennas on a bumpy road: (a) the raw received signal; (b) the envelope of the received signal.

In the experiment, the actual number of breaths counted by the testee in 30 s was 13, while the number of the FSR system was 16. The relative error is  $(16 - 13)/13 = 23.07\%$ . The result shows that the FSR system is sensitive to road conditions. In essence, the problem is due to the random movement of the radar-transmitting antenna, the receiving antenna, the human body, and all the connectors in the system. As shown in Figure 18, we can find that the PVDF system is also influenced by vibration.

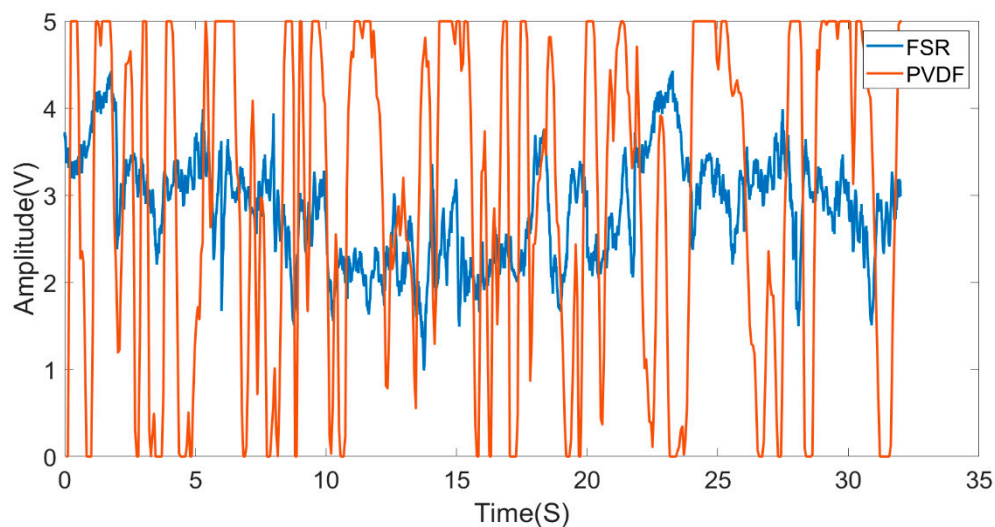


**Figure 18.** The output of the FSR system (blue line) and PVDF system (red line).

#### 4. Conclusions

In the automobile environment, this paper proposes a low-cost yet effective non-contact respiration detection method based on the change of radar cross-section (RCS) for the respiration detection. In our method, the forward-scattering radar (FSR) system is employed to accurately detect the driver's respiratory rate. Compared with other non-contact respiration detection bio-radar, the proposed detection system has a higher comfort level and lower overall cost. The experimental comparison shows great consistency in results and high measurement accuracy. The system uses a directional antenna to reduce the multipath effect and judges the driver's sitting posture by computing the mean of the received signal's envelope. The cost of the FSR system in this paper is 80 dollars. In the future, this technology can be integrated into the car, using the existing WIFI to achieve a system cost of less

than 10 US dollars. For our future work, we will investigate how to reduce the effect of random motion artifacts in the system to further improve the system's robustness on bumpy roads.

**Author Contributions:** F.Y. proposed the idea of this article, designed the experiment setup, and finished the manuscript. S.G. revised the paper. Z.H. led the research project. Y.F. performed experimental results analysis. J.L. designed the hardware system. L.L. performed the antenna simulation. K.J. participated in the experiment with the PVDF system. All authors have read and agreed to the published version of the manuscript.

**Funding:** This work is supported by the Sichuan Province Science and Technology Program Research Project (No.2019YJ0174)

**Conflicts of Interest:** The authors declare no conflict of interest.

**Ethical Statements:** The human protocols used in this work were evaluated and approved by the Ethic Committee of the University of Electronic Science and Technology of China. They are in accordance with Helsinki declaration and the National laws and regulations for "Regulation for ethical review of biomedical research involving human beings".

## References

1. Kim, J.; Shin, M. Utilizing HRV-derived respiration measures for driver drowsiness detection. *Electronics* **2019**, *8*, 669. [[CrossRef](#)]
2. Valderas, M.T.; Bolea, J.; Laguna, P.; Vallverdú, M.; Bailón, R. Human emotion recognition using heart rate variability analysis with spectral bands based on respiration. In Proceedings of the 2015 37th Annual International Conference of the IEEE Engineering in Medicine and Biology Society (EMBC), Milan, Italy, 25–29 August 2015; pp. 6134–6137.
3. Harold, L.; Manning, M.D.; Richard, M.; Schwartzstein, M.D. Respiratory Sensations in Asthma: Physiological and Clinical Implications. *J. Asthma* **2001**, *38*, 447–460.
4. Chen, M.; Tian, Y.; Fortino, G.; Zhang, J.; Humar, I. Cognitive Internet of Vehicles. *Comput. Commun.* **2018**, *120*, 58–70. [[CrossRef](#)]
5. He, X.; Goubran, R.; Knoefel, F. IR night vision video-based estimation of heart and respiration rates. In Proceedings of the 2017 IEEE Sensors Applications Symposium (SAS), Glassboro, NJ, USA, 13–15 March 2017; pp. 1–5.
6. Murthy, R.; Pavlidis, I.; Tsiamyrtzis, P. Touchless monitoring of breathing function. *Annu. Int. Conf. IEEE Eng. Med. Biol. - Proc.* **2004**, *26 II*, 1196–1199.
7. Lu, C.; Yuan, Y.; Tseng, C.H.; Wu, C.T.M. Multi-Target Continuous-Wave Vital Sign Radar using 24 GHz Metamaterial Leaky Wave Antennas. *IEEE MTT-S 2019 Int. Microw. Biomed. Conf. IMBioC 2019 - Proc.* **2019**, *1*, 1–4.
8. Zhang, Y.; Qi, F.; Lv, H.; Liang, F.; Wang, J. Bioradar Technology: Recent Research and Advancements. *IEEE Microw. Mag.* **2019**, *20*, 58–73. [[CrossRef](#)]
9. Fei, J.; Pavlidis, I. Thermistor at a distance: Unobtrusive measurement of breathing. *IEEE Trans. Biomed. Eng.* **2010**, *57*, 988–998. [[PubMed](#)]
10. Fei, J.; Pavlidis, I. Virtual thermistor. In Proceedings of the 2007 29th Annual International Conference of the IEEE Engineering in Medicine and Biology Society, Lyon, France, 22–26 August 2007; pp. 250–253.
11. Sensing, O. EM-Wave Biosensors: A Review of RF, Microwave, mm-Wave and Optical Sensing. *Sensors* **2019**, *19*, 1013. [[CrossRef](#)]
12. Shyu, K.K.; Chiu, L.J.; Lee, P.L.; Tung, T.H.; Yang, S.H. Detection of Breathing and Heart Rates in UWB Radar Sensor Data Using FVPIEF-Based Two-Layer EEMD. *IEEE Sens. J.* **2019**, *19*, 774–784. [[CrossRef](#)]
13. Chen, Y.; Gunawan, E.; Low, K.S.; Soh, C.B.; Thi, L.L. Human respiration rate estimation using body-worn ultra-wideband radar. In Proceedings of the 2007 IEEE Antennas and Propagation Society International Symposium, Honolulu, HI, USA, 9–15 June 2007; pp. 265–268.
14. Prevention, C.C.; Leem, S.K.; Khan, F.; Cho, S.H. Vital Sign Monitoring and Mobile Phone Usage Detection Using IR-UWB Radar for Intended Use in car Crash Prevention. *Sensors* **2017**, *17*, 1240. [[CrossRef](#)]
15. Park, B.; Member, S.; Boric-lubecke, O.; Member, S.; Lubecke, V.M.; Member, S. Arctangent Demodulation With DC Offset Compensation in Quadrature Doppler Radar Receiver Systems. *IEEE Trans. Microw. Theory Tech.* **2007**, *55*, 1073–1079. [[CrossRef](#)]

16. Li, C.; Lin, J. Random body movement cancellation in doppler radar vital sign detection. *IEEE Trans. Microw. Theory Tech.* **2008**, *56*, 3143–3152.
17. Levitas, B.; Matuzas, J. UWB Radar for Breath Detection. In Proceedings of the 11th International Radar Symposium, Vilnius, Lithuania, 16–18 June 2010; pp. 1–3.
18. Schires, E.; Georgiou, P.; Lande, T.S. Vital sign monitoring through the back using an UWB impulse radar with body coupled antennas. *IEEE Trans. Biomed. Circuits Syst.* **2018**, *12*, 292–302. [[CrossRef](#)] [[PubMed](#)]
19. Pisa, S.; Chicarella, S.; Pittella, E.; PiuZZi, E.; Testa, O.; Cicchetti, R. A double-sideband continuous-wave radar sensor for carotid wall movement detection. *IEEE Sens. J.* **2018**, *18*, 8162–8171. [[CrossRef](#)]
20. Wu, C.; Yang, Z.; Zhou, Z.; Liu, X.; Liu, Y.; Cao, J. Non-invasive detection of moving and stationary human with WiFi. *IEEE J. Sel. Areas Commun.* **2015**, *33*, 2329–2342. [[CrossRef](#)]
21. Raja Abdullah, R.S.A.; Rasid, M.F.A.; Mohamed, M.K. Improvement in detection with forward scattering radar. *Sci. China Inf. Sci.* **2011**, *54*, 2660–2672. [[CrossRef](#)]
22. Sun, H. Through-the-Wall Human Motion Sensing Based on Forward Scattering. In Proceedings of the 2019 IEEE Radar Conference (RadarConf), Boston, MA, USA, 22–26 April 2019; pp. 1–5.
23. Yang, F.; He, Z.; Fu, Y.; Li, L.; Jiang, K.; Xie, F. Noncontact detection of respiration rate based on forward scatter radar. *Sensors* **2019**, *19*, 4778. [[CrossRef](#)]
24. Chernyak, V.S. Radar Cross Section (RCS) of Targets. In *Fundamentals of Multisite Radar Systems: Multistatic Radars and Multistatic Radar Systems*, 1st ed.; Routledge: London, UK, 1998; pp. 32–36.
25. Chen, J. Modeling of Near-field Bistatic RCS of Complex Targets. *J. Proj. Guid.* **2010**, *30*, 157–160.
26. Gouveia, C.; Loss, C.; Pinho, P.; Vieira, J. Different antenna designs for non-contact vital signs measurement: A review. *Electronics* **2019**, *8*, 1294. [[CrossRef](#)]
27. Comite, D.; Galli, A.; Catapano, I.; Soldovieri, F. The Role of the Antenna Radiation Pattern in the Performance of a Microwave Tomographic Approach for GPR Imaging. *IEEE J. Sel. Top. Appl. Earth Obs. Remote Sens.* **2017**, *10*, 4337–4347. [[CrossRef](#)]



© 2020 by the authors. Licensee MDPI, Basel, Switzerland. This article is an open access article distributed under the terms and conditions of the Creative Commons Attribution (CC BY) license (<http://creativecommons.org/licenses/by/4.0/>).